




Cite this: *RSC Adv.*, 2024, 14, 1094

Urea-rich porous organic polymer as a hydrogen bond catalyst for Knoevenagel condensation reaction and synthesis of 2,3-dihydroquinazolin-4(1*H*)-ones†

Narges Zarei, Meysam Yarie, * Morteza Torabi and Mohammad Ali Zolfigol *

In this research, a new urea-rich porous organic polymer (urea-rich POP) as a hydrogen bond catalyst was synthesized *via* a solvothermal method. The physiochemical properties of the synthesized urea-rich POP were investigated by using different analyses like Fourier transform infrared (FT-IR) spectroscopy, field-emission scanning electron microscopy (FE-SEM), transmission electron microscopy (TEM), thermogravimetric analysis (TGA), derivative thermogravimetry (DTG), energy-dispersive X-ray spectroscopy (EDS), elemental mapping analysis, X-ray diffraction analysis (XRD) and Brunauer–Emmett–Teller (BET) techniques. The preparation of urea-rich POP provides an efficacious platform for designing unique hydrogen bond catalytic systems. Accordingly, urea-rich POP, due to the existence of several urea moieties as hydrogen bond sites, has excellent performance as a catalyst for the Knoevenagel condensation reaction and multi-component synthesis of 2,3-dihydroquinazolin-4(1*H*)-ones.

Received 7th December 2023
Accepted 14th December 2023

DOI: 10.1039/d3ra08354c

rsc.li/rsc-advances

Introduction

Porous materials due to their prospects for performing many chemical transformations are of significant importance.^{1–3} Among the building blocks of porous materials, porous organic polymers (POPs) are the cornerstone for many research areas such as gas storage and separation, smart chemo sensors, energy storage, catalytic transformations and drug delivery.^{3–10} The bottom-up approach as a unique strategy has been used for the construction of polymeric frameworks by different linkages such as imine, boronate, hydrazone and diazonium which are synthesized from selected structural linkers and monomers.^{11–18} These advanced materials have highly ordered structures, devisable modular nature, large surface areas, tunable pore sizes and good thermal and chemical stability.^{19–21} In this respect, POPs by far are reliable and fantastic representatives for heterogeneous catalysis.²² POPs implement specific conditions to control the nature of catalytic centers. Also, these materials control the placement of surrounding surface-active sites.^{23–28} Evidently, POPs due to their ordered pore channels and excellent porosity are irreplaceable materials as hosts for guests in many catalytic reactions. Moreover, the heterogeneous nature of POP-based catalysts allows them to be easily recovered and reused after performing their catalytic activity.^{29–33}

Urea-linked POPs, as novel series of POPs, are flexible building blocks which exhibit reversible structural dynamics in their framework.³⁴ Hydrogen bond interactions and π – π stacking environments have significant effect on the conformational orientation of urea linkages which in turn affects the morphology of the target polymer.^{34–37} The mentioned items have an important impact on the catalytic activity of these unique systems. Urea-linked POPs can enhance the synergistic reaction strategy with the incorporation of two or more active sites in close proximity to activate the reactants which leads to a decrease in the activation energy barrier.³⁴ Considering the above, POPs, especially urea-linked POPs, are beneficial precursors for many catalytic transformations such as Knoevenagel condensation,³⁸ cross coupling reactions,³⁹ oxidation and reduction reactions,³⁹ asymmetric catalysis,⁴⁰ arylation reactions²⁷ CO₂ fixation,⁴¹ photocatalytic reactions⁴² and multi-component reactions.⁴³

Knoevenagel condensation, as a forefront and fundamental reaction for C=C bond formation, is an important reaction to achieving carbohydrates, fragrances, herbicides and dyes. Generally, Knoevenagel adducts are constructed by the reaction between aldehydes or ketones and compounds which contain acidic methylene bridges.^{44–47} Nonetheless, the preparation of these compounds using POPs is of great interest.^{48–50} Secondly, quinazolinone families are valuable assortment of nitrogen-containing heterocyclic compounds which are abundantly used in the pharmaceutical communities. There are several valuable marketed drugs in which quinazolinone moieties are involved.^{51–54} Numerous medicinal properties such as

Department of Organic Chemistry, Faculty of Chemistry and Petroleum Sciences, Bu-Ali Sina University, Hamedan, Iran. E-mail: myarie.5266@gmail.com; zolfigol@basu.ac.ir; mzolfigol@yahoo.com

† Electronic supplementary information (ESI) available. See DOI: <https://doi.org/10.1039/d3ra08354c>



anticonvulsant, anticancer, hypolipidemic, antimalarial, anti-diabetic and activities have been reported for these compounds.^{55–57}

Our initial perspective is the design and synthesis of a new urea-rich POP and it was applied as an unique heterogeneous hydrogen bond catalyst for Knoevenagel condensation reaction and synthesis of 2,3-dihydroquinazolin-4(1*H*)-ones (Schemes 1 and 2).

Results and discussion

Because of the effective role of catalysts in the chemical and industrial processes, development of catalytic systems for the organic transformations is one of the main research demands. In continuation of our investigation on the synthesis of dihydroquinolines,^{58–62} herein, we decided to synthesize a new urea-rich POP as a hydrogen bond catalyst for the Knoevenagel condensation reaction and preparation of 2,3-dihydroquinazolin-4(1*H*)-ones.

Support for the proposed chemical structure of urea-rich POP came from FT-IR analysis. In this respect, FT-IR spectra of the resulting urea-rich POP and its related starting materials were depicted in Fig. 1. FT-IR spectrum of tris(4-aminophenoxy)-1,3,5-triazine (**TAPT**) shows stretching vibrations characteristic of NH₂ groups at 3379 and 3469 cm⁻¹. The characteristic peak of C=N bonds appeared in the area of 1610 cm⁻¹. According to the FT-IR spectrum of bis(4-isocyanatophenyl)methane (**BICPM**), the sharp signal in the areas of 2263 cm⁻¹ is related to isocyanate groups. After the polymerization reaction (to give urea-rich POP), the vibrational mode of isocyanate groups of **BICPM** and NH₂ of **TAPT** disappeared. Meanwhile, appearance of a new peak at 1669 cm⁻¹, can be attributed to the amidic carbonyl groups stretching mode. In addition, signal of the amidic N–H groups has been appeared at 3339 cm⁻¹ which in turn in a strong reason for the confirmation of the successful synthesis of urea-rich POP (Fig. 1).

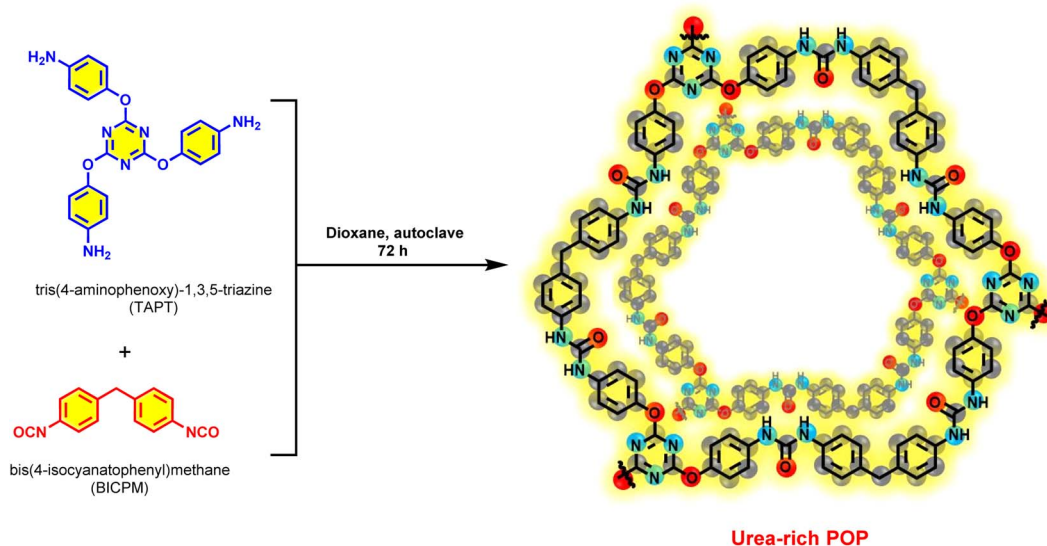
Result of the EDS analysis was confirmed the presence of C, O and N elements. Additionally, mapping analysis was used for the determination of the uniform scattering of desired elements. Elemental mapping images of urea-rich POP revealed that the N, O and C are distributed homogeneously in the urea-rich POP (Fig. 2).

In order to investigate the surface morphology of the prepared urea-rich POP, FE-SEM analysis was used. According to FE-SEM images of urea-rich POP, the porous organic polymer has a morphology of intertwined threads spheres (Fig. 3a and b). Additionally, TEM analysis has been applied to further study of urea-rich POP morphology. From the TEM images of urea-rich POP (Fig. 3c–e), it was clearly observed that the described catalyst has regular spheres stuck together containing particles with different sizes (from nanometer to micrometer).

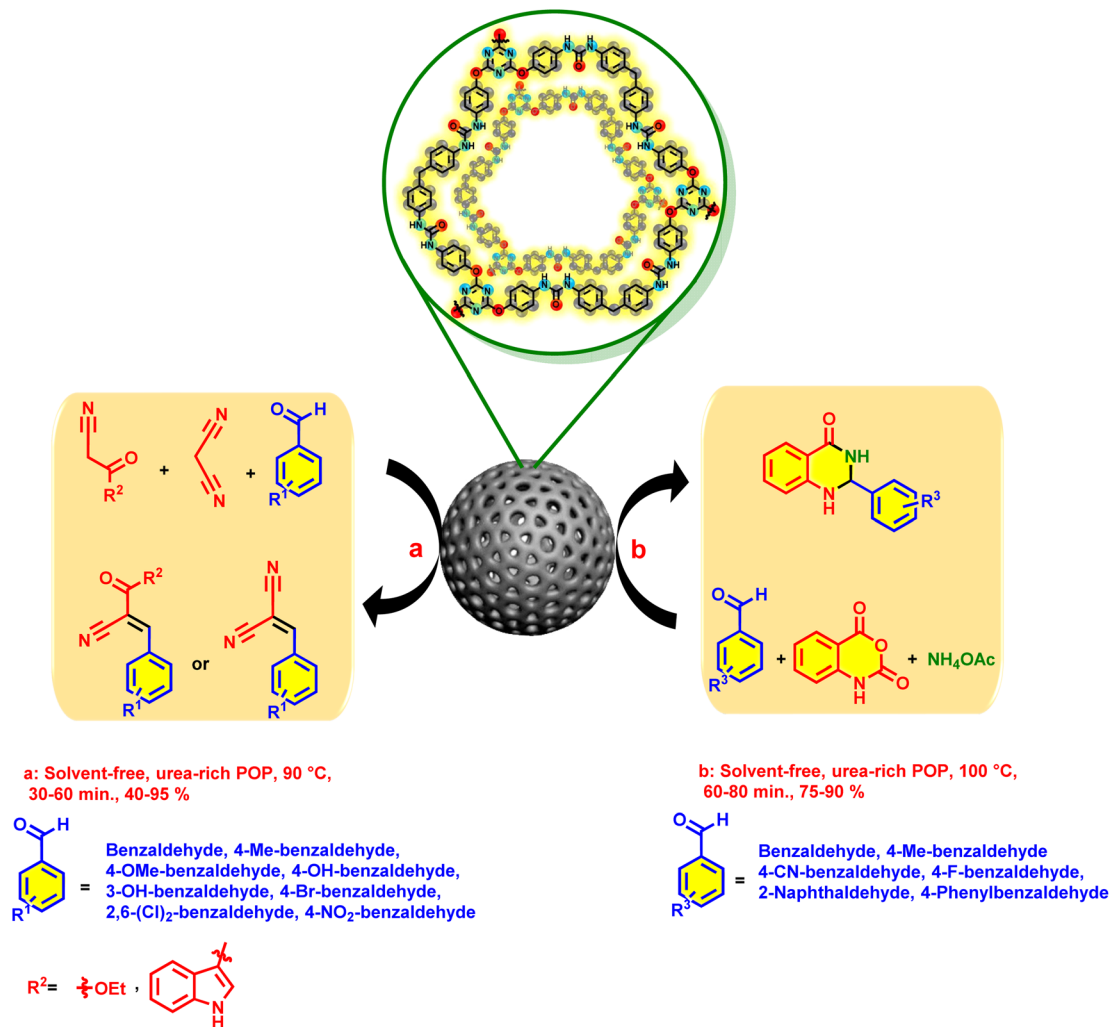
In another study, the synthesized catalyst was characterized by nitrogen adsorption/desorption measurements at 77 K (Fig. 4a). The adsorption isotherm belongs to the type III isotherm of IUPAC classification. The appearance of hysteresis loops reveals the existence of mesopores in the synthesized catalyst. The specific surface area of urea-rich POP is 47 m² g⁻¹ which clearly shows the good porosity of urea-rich POP. Also, the pore size distribution curves, derived from BJH analysis, demonstrated that the size of most of the pores for urea-rich POP are in range of 2–30 nm (Fig. 4b), revealing the presence of mesopores.

XRD pattern illustrated that urea-rich POP has sharp signals at 21°, 29°, 36°, 39°, 43°, 47° and 49°. With more precision, the broad diffraction peak about 2θ = 21°, is attributable to the π–π stacking of the aromatic building blocks. Other sharp peaks prove that catalyst has a relatively order crystalline structure (Fig. 5).

TGA/DTG analyses as a conventional method were used for the determination of thermal stability of urea-rich POP. According to TGA/DTG curves of urea-rich POP (Fig. 6), a major weight loss occurred about at 340 °C, while a negligible weight loss was observed before this temperature and this verified the excellent thermal stability of catalyst.



Scheme 1 Experimental route for the synthesis of urea-rich POP.



Scheme 2 General procedure for the catalytic synthesis of Knoevenagel adducts and 2,3-dihydroquinazolin-4(1H)-ones.

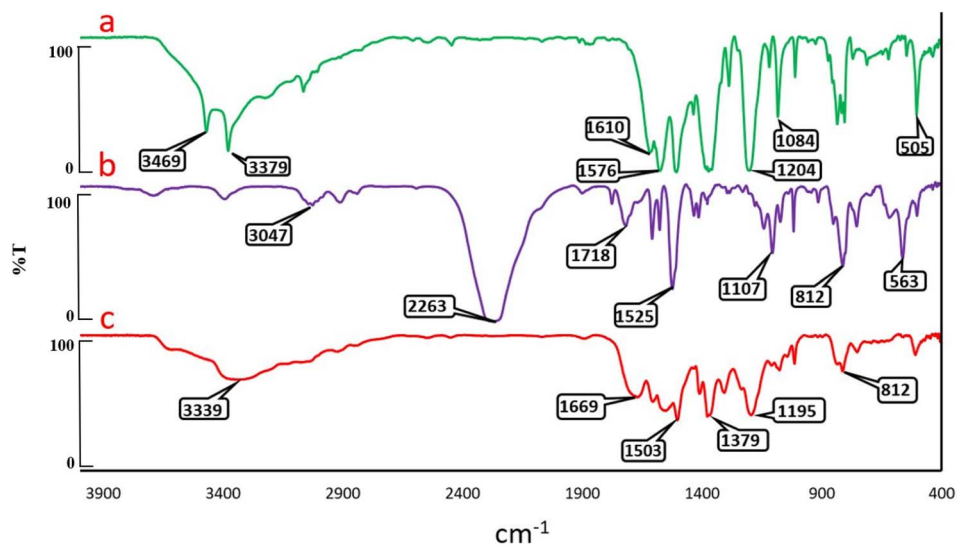


Fig. 1 FT-IR spectra of TAPT (a), BICPM (b) and urea-rich POP (c).



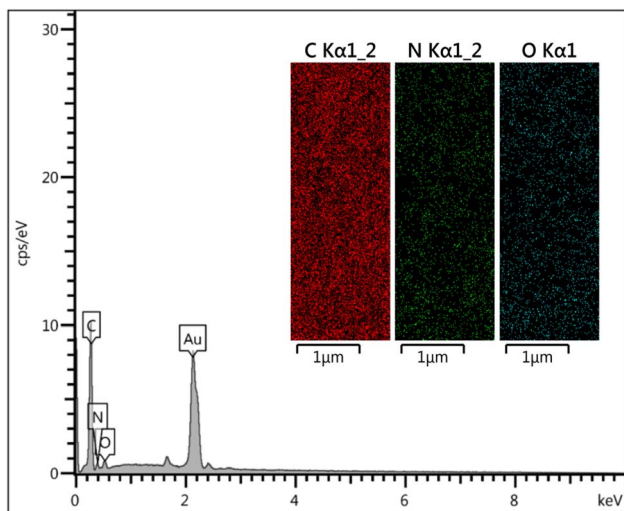


Fig. 2 EDS and elemental mapping analyses of urea-rich POP.

In the following, we have focused on the investigation of catalytic behavior of urea-rich POP as a hydrogen bond catalyst for the Knoevenagel condensation reaction and multi-component synthesis of 2,3-dihydroquinazolin-4(1*H*)-ones. In this regard, the required reactions were carried out to find the optimal conditions for the Knoevenagel condensation reaction and 2,3-dihydroquinazolin-4(1*H*)-ones synthesizing. At first, 4-hydroxy benzaldehyde and malononitrile as model substrates and urea-rich POP as a catalyst were selected for optimization of the reaction conditions for the synthesis of related Knoevenagel adduct. For exploration of the impact of temperature, the model reaction was performed at different

temperatures by using 20 mg of catalyst. The resulting data indicated that the 90 °C is the best temperature for the reaction. Then, the model reaction was performed at 90 °C in the presence of different amounts of the catalyst (10, 15 and 20 mg). The obtained data confirmed that 20 mg of catalyst is the best of choice. Also, the model reaction was done in H₂O and several organic solvents and also, solvent free conditions. It was found that the selected solvents did not provide suitable conditions for the progress of the reaction. Furthermore, the reaction was also done in the absence of catalyst under solvent free conditions, which did not progress sufficiently. Considering the obtained data, the optimal reaction conditions is where the model reaction performed under solvent free conditions by using 20 mg of catalyst at the 90 °C (Table 1). Similarly, we delve into the screening of optimal reaction conditions for the preparation of 2,3-dihydroquinazolin-4(1*H*)-ones. It was found that stirring at 100 °C by using 20 mg of urea-rich POP as a catalyst for 60 min without any solvent affords the best yield (90%) (Table 2).

The archived data from the catalytic performance of urea-rich POP in the Knoevenagel reaction and synthesis of 2,3-dihydroquinazolin-4(1*H*)-ones encouraged us to investigate the generality of the catalytic activity. In the section of Knoevenagel reaction, a series of aldehydes with different electron-deficient and electron-rich aromatic substituents were tested. Also, malononitrile, ethyl cyanoacetate and 3-(1*H*-indol-3-yl)-3-oxopropanenitrile were used as compounds which contain acidic methylene bridge. All the aldehydes and CH-acid compounds, provide the corresponding products with high yields at short reaction times (Table 3). Various aldehydes were also used for the preparation of 2,3-

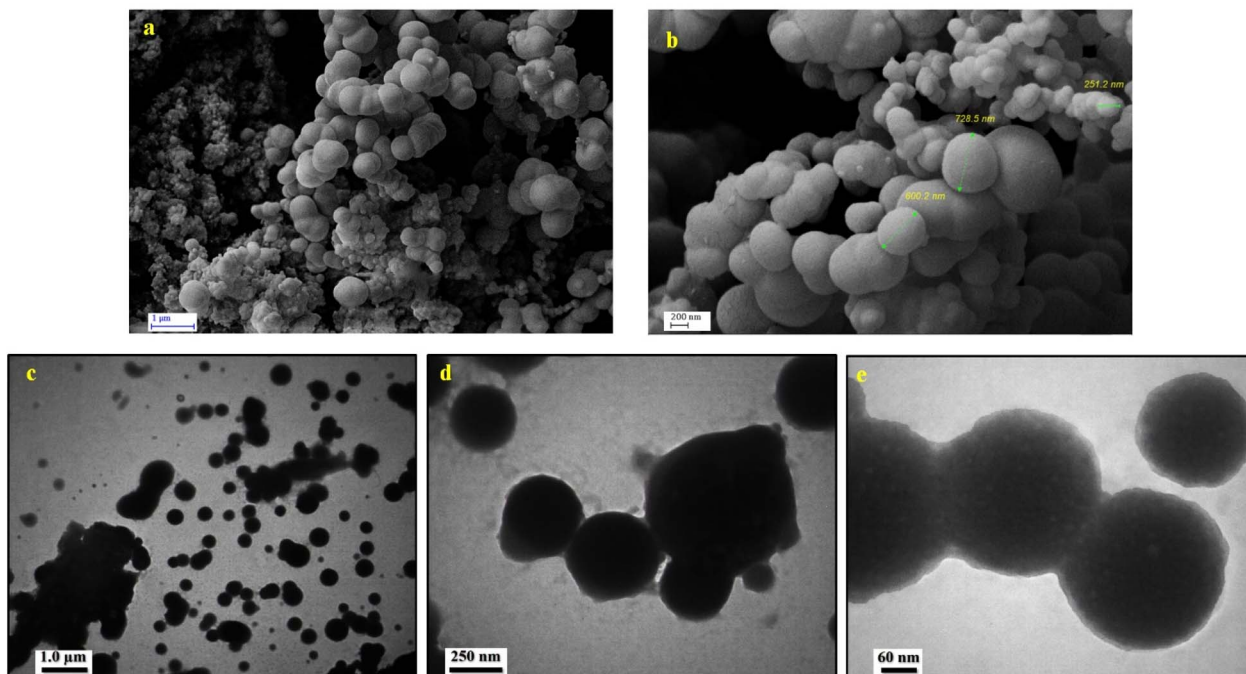


Fig. 3 FE-SEM images of urea-rich POP (a and b) and TEM images of urea-rich POP (c–e).

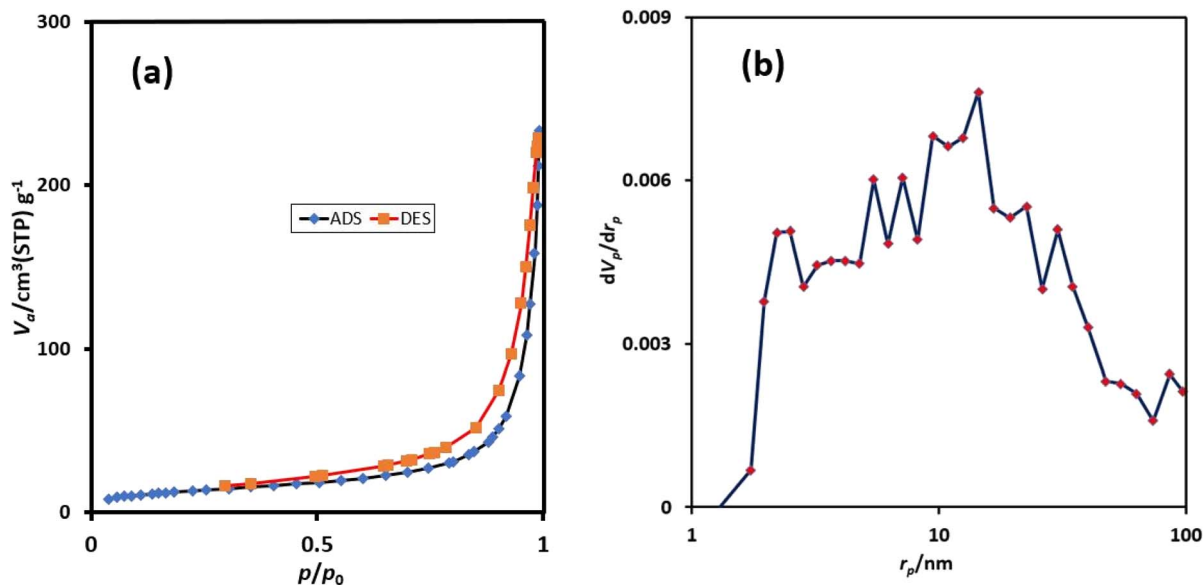


Fig. 4 The N_2 adsorption-desorption isotherms of urea-rich POP (a) and pore size distribution curves of urea-rich POP (b).

dihydroquinazolin-4(1*H*)-ones. In this case, the synthesized derivatives had high yields and short reaction times (Table 3).

In another study, in order to find out the role of the desired catalyst, the model reactions, was checked out in the presence of urea and thiourea for comparison. The results indicated that the synthesized catalyst has the better performance. Also, due to the heterogeneity of the target catalyst, it is easily separated from the mixture of reaction and can be reused. It is worth noting that the two mentioned catalysts are homogeneous and it is not easy to separate them from the reaction mixture (Tables 4 and 5).

Besides characteristic parameters and catalytic activity, recovering and reusing of urea-rich POP as one of the influential parameters of heterogeneous catalysts was studied. To our delight, when the model reaction for Knoevenagel condensation was performed at the obtained optimum reaction conditions, the catalyst could be used at least 5 times with a negligible decreasing in catalytic activity and yield of product (Scheme 3). Hence, after accomplishing

the model reaction in each run, the mixture of reaction was dissolved in 30 mL hot EtOH while the catalyst is insoluble. Accordingly, the catalyst was easily separated by using filter paper, washed with EtOH, dried and retained for the next reaction. Also, the stability of the recovered catalyst was investigated by FT-IR spectroscopy (see ESI†).

In another exploration, we suggested a mechanistic route for the preparation of **2f** as follows. At first, ammonia derived from the dissociation of ammonium acetate attack to catalytic activated isatoic anhydride which leads to intermediate A. Then, *via* a CO_2 releasing process, intermediate A was converted to intermediate B. In the next step, aldehyde was activated by the catalyst and reacted with intermediate B to generate intermediate C. After that, the desired product was performed through an intramolecular nucleophilic attack (Scheme 4).

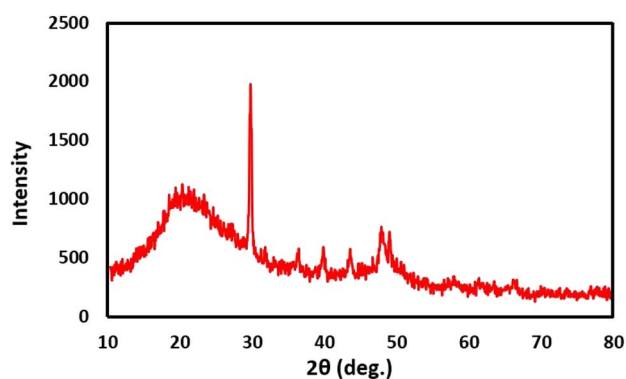


Fig. 5 XRD pattern of urea-rich POP.

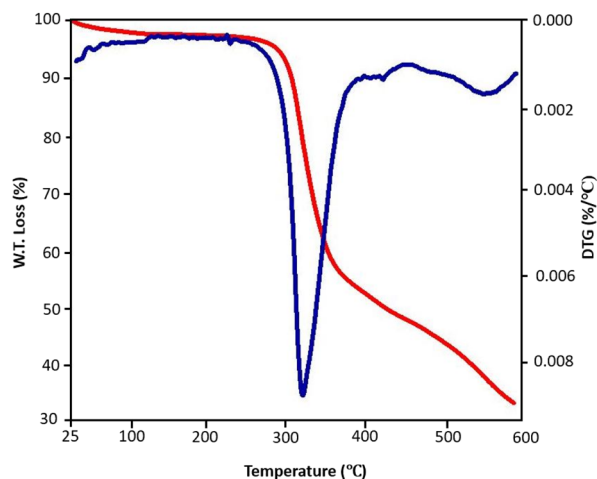
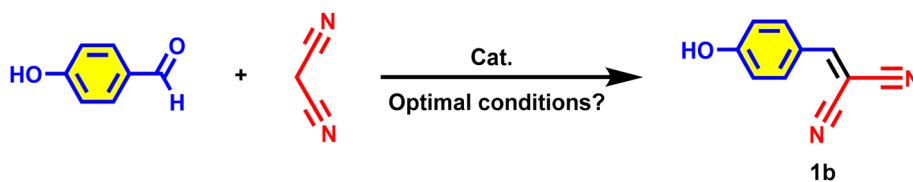


Fig. 6 TGA/DTG curves of urea-rich POP.



Table 1 Optimization of reaction conditions for synthesis of **1b**^a

Entry	Solvent	Temperature (°C)	Catalyst loading (mg)	Time (min)	Yield ^b (%)
1	—	100	20	30	95
2 ^c	—	90	20	30	95
3	—	90	15	30	90
4	—	90	10	60	70
5	—	90	—	120	30
6	—	80	20	60	20
7	—	80	20	240	40
8	H ₂ O	Reflux	20	60	—
9	EtOH	Reflux	20	60	—
10	<i>n</i> -Hexane	Reflux	20	60	—
11	EtOAc	Reflux	20	60	—
12	CH ₂ Cl ₂	Reflux	20	60	—

^a Reaction conditions: malononitrile (1 mmol, 0.066 g), 4-hydroxybenzaldehyde (1 mmol, 0.122 g). ^b Isolated yields. ^c Optimal data.

Experimental section

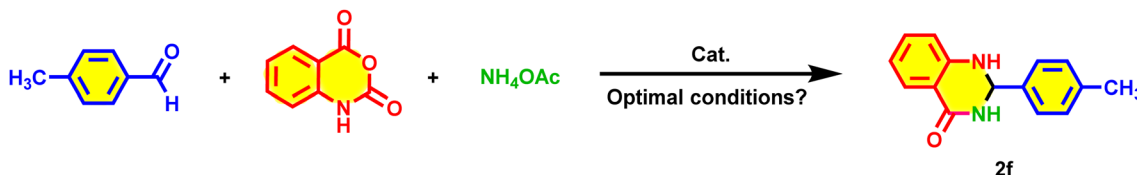
General procedure for the synthesis of urea-rich POP

Initially, TAPT was synthesized according to the previously reported methods.⁷⁷ Then, a mixture of TAPT (0.4 mmol, 0.16 g), BICPM (0.65 mmol, 0.16 g) and dioxane (6 mL) were sealed in a 25 mL Teflon lined stainless steel vessel and heated at 110 °C for 72 h. After completing the reaction, the obtained light brown precipitate

was washed three times with hot THF, MeOH and CH₂Cl₂. Finally, the obtained precipitate was dried for 12 h at 80 °C.

Experimental procedure for Knoevenagel condensation reaction by using urea-rich POP as catalyst

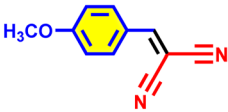
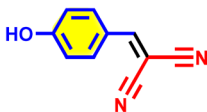
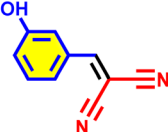
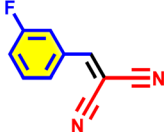
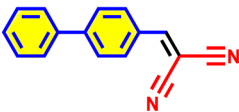
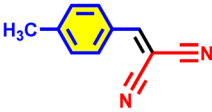
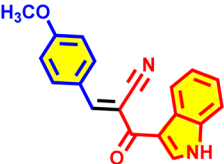
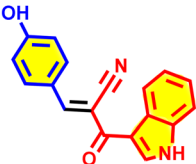
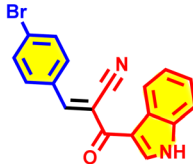
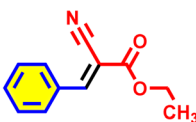
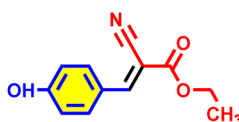
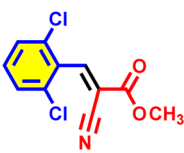
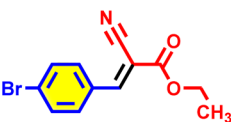
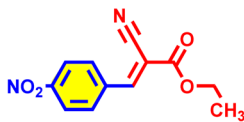
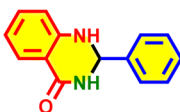
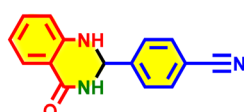
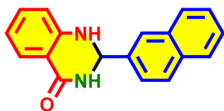
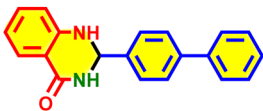
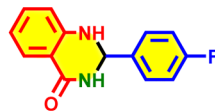
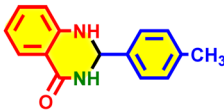
Aryl aldehydes (1 mmol), malononitrile (1 mmol, 0.066 g) or ethyl cyanoacetate (1 mmol, 0.113 g) or 3-(1*H*-indol-3-yl)-3-

Table 2 Optimization of reaction conditions for synthesis of **2f**^a

Entry	Solvent	Temperature (°C)	Catalyst loading (mg)	Time (min)	Yield ^b (%)
1 ^c	—	100	20	60	90
2	—	100	15	90	80
3	—	100	10	100	65
4	—	90	20	80	78
5	—	100	—	120	70
6	—	80	20	180	70
7	—	70	20	240	40
8	H ₂ O	Reflux	20	60	Trace
9	EtOH	Reflux	20	60	50
10	<i>n</i> -Hexane	Reflux	20	60	—
11	MeOH	Reflux	20	60	45
12	CH ₂ Cl ₂	Reflux	20	60	—

^a Reaction conditions: 4-methylbenzaldehyde (1 mmol, 0.12 g), isatoic anhydride (1 mmol, 0.163 g), ammonium acetate (3 mmol, 0.231 g). ^b Isolated yields. ^c Optimal data.

Table 3 Preparation of Knoevenagel-based compounds (1a–1n) and preparation of dihydroquinazolin-4(1*H*)-one derivatives (2a–2f) in the presence of urea-rich POP as catalyst^a

 <p>1a, 45 min., 80% M.p.: 115-117 °C [112-114]⁶³</p>	 <p>1b, 30 min., 95% M.p.: 181-182 °C [184-186]⁶⁴</p>	 <p>1c, 40 min., 80% M.p.: 150-151 °C [152-154]⁶⁴</p>	 <p>1d, 30 min., 92% M.p.: 85-86 °C [93-94]⁶⁵</p>
 <p>1e, 30 min., 90% M.p.: 144-146 °C [144]⁶⁶</p>	 <p>1f, 30 min., 95% M.p.: 132-135 °C [132-134]⁶⁴</p>	 <p>1g, 50 min., 40% M.p.: 244-246 °C [256-258]⁶⁷</p>	 <p>1h, 50 min., 50% M.p.: 250-252 °C [252-253]⁶⁷</p>
 <p>1i, 60 min., 60% M.p.: 219-221 °C [221-223]⁶⁸</p>	 <p>1j, 30 min., 95% M.p.: 50-51 °C [56-58]⁶⁹</p>	 <p>1k, 30 min., 92% M.p.: 162-164 °C [170]⁷⁰</p>	 <p>1l, 40 min., 75% M.p.: 68-70 °C [70-73]⁷¹</p>
 <p>1m, 30 min., 84% M.p.: 83-85 °C [85-86]⁷⁰</p>	 <p>1n, 45 min., 90% M.p.: 150-153 °C [165-167]⁶⁹</p>	 <p>2a, 70 min., 85% M.p.: 224-226 °C [218-220]⁷²</p>	 <p>2b, 70 min., 75% M.p.: 172-174 °C [178-180]⁷³</p>
 <p>2c, 70 min., 86% M.p.: 217-219 °C [216]⁷⁴</p>	 <p>2d, 80 min., 80% M.p.: 222-223 °C [217-218]⁷⁵</p>	 <p>2e, 60 min., 88% M.p.: 196-198 °C [195-197]⁷⁶</p>	 <p>2f, 60 min., 90% M.p.: 227-229 °C [230-232]⁷⁶</p>

^a Reaction conditions for the preparation of Knoevenagel-based compounds: aldehyde (1 mmol), CH-acid compound (1 mmol), and urea-rich POP (20 mg), solvent-free, 90 °C. Reaction conditions for the preparation of dihydroquinazolin-4(1*H*)-one derivatives: aldehyde (1 mmol), isatoic anhydride (1 mmol, 0.163 g), ammonium acetate (3 mmol, 0.231 g) and urea-rich POP (20 mg), solvent-free, 100 °C, reported yields are referred to isolated yields.

oxopropanenitrile (1 mmol, 0.184 g) and urea-rich POP (0.02 g) were mixed in a round bottom flask without using any solvent and were stirred by a heater stirrer at 90 °C. TLC technique was used for the assignment of the precession of the reaction. After the reaction time is over, 30 mL of hot

EtOH was added to the reaction composition and all of the materials were dissolved in EtOH and the insoluble catalyst was removed by filter paper. After that, the desired products were treated with 10 mL of cold EtOH and easily purified and dried for a sufficient time at 25 °C to yield the pure products.



Table 4 Comparison of the catalytic performance of urea-rich POP and two other formal catalysts for the synthesis of **1b**^a

Entry	Catalyst	The amount of catalyst	Yield (%)
1	Urea-rich POP	20 mg	95
2	Urea	10 mol%	Trace
3	Thiourea	10 mol%	25

^a Reaction conditions: malononitrile (1 mmol, 0.066 g), 4-hydroxybenzaldehyde (1 mmol, 0.122 g), solvent-free, 90 °C, 30 min.

Table 5 Comparison of the catalytic performance of urea-rich POP and two other formal catalysts for the synthesis of **2f**^a

Entry	Catalyst	The amount of catalyst	Yield (%)
1	Urea-rich POP	20 mg	90
2	Urea	10 mol%	45
3	Thiourea	10 mol%	20

^a Reaction conditions: 4-methylbenzaldehyde (1 mmol, 0.12 g), isatoic anhydride (1 mmol, 0.163 g), ammonium acetate (3 mmol, 0.231 g), solvent-free, 100 °C, 60 min.

Experimental route for preparation of dihydroquinazolin-4(1H)-one derivatives by applying urea-rich POP as catalyst

Aromatic aldehyde families (1 mmol), isatoic anhydride (1 mmol, 0.163 g), ammonium acetate (3 mmol, 0.231 g) and urea-rich POP (20 mg) were mixed in a round bottom flask and reacted without using any solvent at 100 °C. The precession of the reaction was monitored by using TLC techniques. After completing each reaction, 30 mL of CH₂Cl₂ was added to the reaction mixture and all of the materials except the used catalyst were dissolved in CH₂Cl₂. After that, the catalyst was easily separated by using a filtration process, the solvent was removed and the remaining solid was treated to 10 mL of cold EtOH and easily purified. Finally, the obtained products were desiccated at 80 °C.

Spectral data

2-(4-Hydroxybenzylidene)malononitrile (1b). Mp 181–182 °C, FT-IR (KBr, ν , cm⁻¹): 3353, 3080, 2922, 2226, 1610, 1580, 1517. ¹H NMR (301 MHz, DMSO-d₆) δ_{ppm} 11.05 (s, 1H), 8.32 (s, 1H),

7.90 (d, J = 9 Hz, 2H), 7.00 (d, J = 9 Hz, 2H). ¹³C NMR (76 MHz, DMSO-d₆) δ_{ppm} 164.5, 161.0, 134.4, 123.2, 117.1, 115.6, 114.7, 75.4.

2-(3-Fluorobenzylidene)malononitrile (1d). Mp 85–86 °C, FT-IR (KBr, ν , cm⁻¹): 3080, 3040, 2228, 1596, 1573, 1491. ¹H NMR (301 MHz, DMSO-d₆) δ_{ppm} 8.59 (s, 1H), 7.83–7.68 (m, 3H), 7.63–7.56 (m, 1H). ¹³C NMR (76 MHz, DMSO-d₆) δ_{ppm} 164.0, 160.6, 133.8, 132.3, 127.1, 121.7, 117.0, 114.4, 113.3, 84.0.

2-([1,1'-Biphenyl]-4-ylmethylene)malononitrile (1e). Mp 144 °C, FT-IR (KBr, ν , cm⁻¹): 3063, 3030, 2224, 1605, 1576, 1547. ¹H NMR (301 MHz, DMSO-d₆) δ_{ppm} 8.60 (s, 1H), 8.09 (d, J = 9 Hz, 2H), 8.00 (d, J = 9 Hz, 2H), 7.83 (d, J = 9 Hz, 2H), 7.58–7.48 (m, 3H). ¹³C NMR (76 MHz, DMSO-d₆) δ_{ppm} 161.3, 146.1, 138.7, 131.8, 130.8, 129.7, 129.4, 128.0, 127.6, 114.9, 114.0, 81.2.

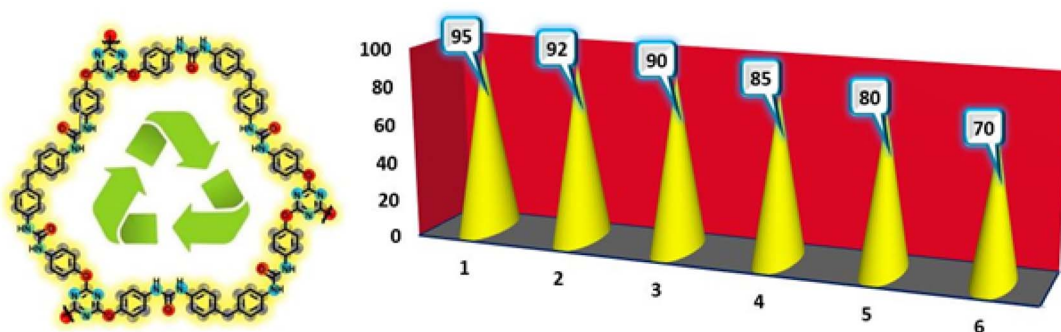
2-(4-Methylbenzylidene)malononitrile (1f). Mp 132–135 °C, FT-IR (KBr, ν , cm⁻¹): 3035, 2968, 2224. ¹H NMR (301 MHz, DMSO-d₆) δ_{ppm} 8.49 (s, 1H), 7.87 (d, J = 9 Hz, 2H), 7.45 (d, J = 6 Hz, 2H), 2.42 (s, 3H). ¹³C NMR (76 MHz, DMSO-d₆) δ_{ppm} 161.8, 146.2, 131.2, 130.6, 129.2, 114.9, 113.9, 80.4, 22.0.

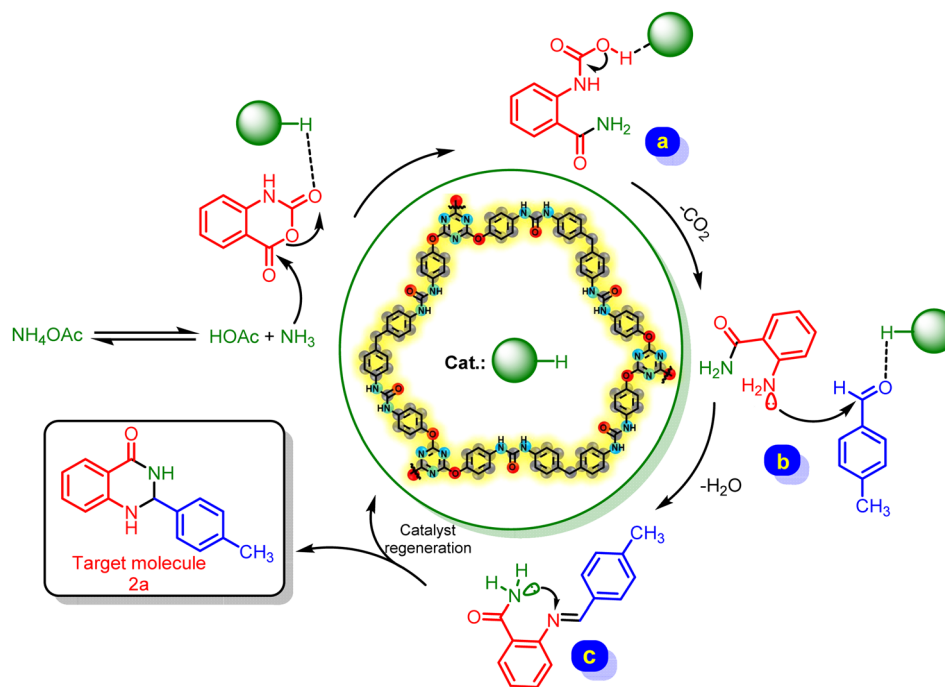
Ethyl (E)-2-cyano-3-(4-hydroxyphenyl)acrylate (1k). Mp 162–164 °C, FT-IR (KBr, ν , cm⁻¹): 3278, 2986, 2229, 1721. ¹H NMR (301 MHz, DMSO-d₆) δ_{ppm} 10.87 (s, 1H), 8.24 (s, 1H), 8.01 (d, J = 9 Hz, 2H), 6.97 (d, J = 9 Hz, 2H), 4.30 (q, J = 9 Hz, 2H), 1.31 (t, J = 6 Hz, 3H). ¹³C NMR (76 MHz, DMSO-d₆) δ_{ppm} 163.5, 163.1, 155.2, 134.5, 122.1, 116.1, 116.9, 97.5, 62.4, 14.5.

(E)-3-(4-Bromophenyl)-2-cyanoacrylate (1m). Mp 83–85 °C, FT-IR (KBr, ν , cm⁻¹): 3035, 2988, 2900, 2223, 1723. ¹H NMR (301 MHz, DMSO-d₆) δ_{ppm} 8.42 (s, 1H), 8.01 (d, J = 9 Hz, 2H), 7.85 (d, J = 9 Hz, 2H), 4.35 (q, J = 6 Hz, 2H), 1.33 (t, J = 9 Hz, 3H). ¹³C NMR (76 MHz, DMSO-d₆) δ_{ppm} 162.1, 154.4, 133.0, 132.9, 131.0, 127.7, 115.9, 103.8, 63.0, 14.5.

2-(Naphthalen-2-yl)-2,3-dihydroquinazolin-4(1H)-one (2c). Mp 217–219 °C, FT-IR (KBr, ν , cm⁻¹): 3281, 3185, 3063, 1648. ¹H NMR (301 MHz, DMSO-d₆) δ_{ppm} 8.41 (s, 1H), 7.99–7.93 (m, 4H), 7.74–7.65 (m, 2H), 7.57–7.54 (m, 2H), 7.31–7.23 (m, 2H), 6.79 (d, J = 6 Hz, 1H), 6.75–6.67 (m, 1H), 5.96 (s, 1H). ¹³C NMR (76 MHz, DMSO-d₆) δ_{ppm} 164.1, 148.4, 139.3, 133.8, 133.5, 133.0, 128.6, 128.5, 128.1, 127.9, 126.9, 126.9, 126.4, 125.3, 117.7, 115.4, 114.9, 67.3.

2-([1,1'-Biphenyl]-4-yl)-2,3-dihydroquinazolin-4(1H)-one (2d). Mp 222–223 °C, FT-IR (KBr, ν , cm⁻¹): 3291, 3189, 3060, 1653. ¹H NMR (301 MHz, DMSO-d₆) δ_{ppm} 8.60 (s, 1H), 8.08 (d, J = 9 Hz,

**Scheme 3** Recovering and reusability test of urea-rich POP in the preparation of **1b**.



Scheme 4 A plausible mechanism for the preparation of **2f** in the presence of urea-rich POP as catalyst.

2H), 7.99 (d, $J = 9$ Hz, 2H), 7.83 (d, $J = 9$ Hz, 2H), 7.58–7.48 (m, 3H). ^{13}C NMR (76 MHz, DMSO-d_6) δ_{ppm} 164.1, 148.3, 141.3, 140.8, 140.2, 133.8, 129.4, 128.1, 127.9, 127.9, 127.2, 127.1, 117.6, 115.5, 114.9, 66.7.

2-(p-Tolyl)-2,3-dihydroquinazolin-4(1H)-one (2f). Mp 227–229 °C, FT-IR (KBr, ν , cm^{-1}): 3313, 3195, 3062, 2931, 1658. ^1H NMR (301 MHz, DMSO-d_6) δ_{ppm} 8.26 (s, 1H), 7.63 (d, $J = 9$ Hz, 1H), 7.40 (d, $J = 9$ Hz, 2H), 7.28–7.20 (m, 3H), 7.08 (s, 1H), 6.77–6.66 (m, 2H), 5.73 (s, 1H), 2.31 (s, 3H). ^{13}C NMR (76 MHz, DMSO-d_6) δ_{ppm} 164.1, 148.4, 139.1, 138.2, 133.7, 129.3, 127.8, 127.3, 117.5, 115.5, 114.9, 66.8, 21.2.

Conclusion

In conclusion, we have described the synthesis of novel urea-rich POP by urea linkers *via* solvothermal conditions. This polymer was precisely characterized by several techniques such as FT-IR, FE-SEM, TEM, EDS, mapping, XRD, TGA/DTG and BET techniques. Also, the catalytic behavior of the prepared structure was investigated in Knoevenagel condensation reaction and preparation of 2,3-dihydroquinazolin-4(1H)-ones. Plentiful hydrogen-bonding interactions of catalyst by starting materials lead to providing the activation energy of the target reactions. Most of prepared molecules have a good yields and short reaction times. In addition, recovering and reusing of urea-rich POP was studied in Knoevenagel condensation reaction and easily used at least 5 times with a negligible decreasing in catalytic activity and yield of product.

Conflicts of interest

There are no conflicts to declare.

Acknowledgements

We thank the Bu-Ali Sina University for financial support to our research group.

References

- 1 J. S. M. Lee and A. I. Cooper, Advances in conjugated microporous polymers, *Chem. Rev.*, 2020, **120**, 2171–2214.
- 2 S. Das, P. Heasman, T. Ben and S. Qiu, Porous organic materials: strategic design and structure–function correlation, *Chem. Rev.*, 2017, **117**, 1515–1563.
- 3 J. Guo and D. Jiang, Covalent organic frameworks for heterogeneous catalysis: principle, current status, and challenges, *ACS Cent. Sci.*, 2020, **6**, 869–879.
- 4 Z. Xiang and D. Cao, Porous covalent–organic materials: synthesis, clean energy application and design, *J. Mater. Chem. A*, 2013, **1**, 2691–2718.
- 5 S. Kramer, N. R. Bennedsen and S. Kegnaes, Porous organic polymers containing active metal centers as catalysts for synthetic organic chemistry, *ACS Catal.*, 2018, **8**, 6961–6982.
- 6 N. Kundu and S. Sarkar, Porous organic frameworks for carbon dioxide capture and storage, *J. Environ. Chem. Eng.*, 2021, **9**, 105090.
- 7 R. R. Liang and X. Zhao, Heteropore covalent organic frameworks: a new class of porous organic polymers with well-ordered hierarchical porosities, *Org. Chem. Front.*, 2018, **5**, 3341–3356.
- 8 Z. J. Lin, J. Lü, L. Li, H. F. Li and R. Cao, Defect porous organic frameworks (dPOFs) as a platform for chiral organocatalysis, *J. Catal.*, 2017, **355**, 131–138.



- 9 Q. Sun, Y. Tang, B. Aguila, S. Wang, F. S. Xiao, P. K. Thallapally and S. Ma, Reaction environment modification in covalent organic frameworks for catalytic performance enhancement, *Angew. Chem., Int. Ed.*, 2019, **58**, 8670–8675.
- 10 M. C. Scicluna and L. Vella-Zarb, Evolution of nanocarrier drug-delivery systems and recent advancements in covalent organic framework–drug systems, *ACS Appl. Nano Mater.*, 2020, **3**, 3097–3115.
- 11 T. He, C. Yang, Y. Chen, N. Huang, S. Duan, Z. Zhang and D. Jiang, Bottom-Up Interfacial Design of Covalent Organic Frameworks for Highly Efficient and Selective Electrocatalysis of CO₂, *Adv. Mater.*, 2022, **34**, 2205186.
- 12 S. Li, R. Ma, S. Xu, T. Zheng, H. Wang, G. Fu and T. Zhang, Two-Dimensional Benzobisthiazole-Vinylene-Linked Covalent Organic Frameworks Outperform One-Dimensional Counterparts in Photocatalysis, *ACS Catal.*, 2023, **13**, 1089–1096.
- 13 P. Pacholak, K. Gontarczyk, R. Kamiński, K. Durka and S. Luliński, Boronate covalent and hybrid organic frameworks featuring P^{III} and P=O Lewis base sites, *Chem.–Eur. J.*, 2020, **26**, 12758–12768.
- 14 K. Gottschling, L. Stegbauer, G. Savasci, N. A. Prisco, Z. J. Berkson, C. Ochsenfeld and B. V. Lotsch, Molecular insights into carbon dioxide sorption in hydrazone-based covalent organic frameworks with tertiary amine moieties, *Chem. Mater.*, 2019, **31**, 1946–1955.
- 15 G. Ji, Z. Yang, H. Zhang, Y. Zhao, B. Yu, Z. Ma and Z. Liu, Hierarchically mesoporous o-hydroxyazobenzene polymers: synthesis and their applications in CO₂ capture and conversion, *Angew. Chem.*, 2016, **128**, 9837–9841.
- 16 D. Zhao and X. Feng, A Special Collection on 2D Materials and Their Applications, *Chem.–Asian J.*, 2021, **16**, 4009.
- 17 Y. Zhi, Z. Wang, H. L. Zhang and Q. Zhang, Recent progress in metal-free covalent organic frameworks as heterogeneous catalysts, *Small*, 2020, **16**, 2001070.
- 18 A. Atılgan, M. M. Cetin, J. Yu, Y. Beldjoudi, J. Liu, C. L. Stern and J. T. Hupp, Post-synthetically elaborated BODIPY-based porous organic polymers (POPs) for the photochemical detoxification of a sulfur mustard simulant, *J. Am. Chem. Soc.*, 2020, **142**, 18554–18564.
- 19 C. Krishnaraj, H. S. Jena, K. Leus and P. Van Der Voort, Covalent triazine frameworks—a sustainable perspective, *Green Chem.*, 2020, **22**, 1038–1071.
- 20 M. Yu, N. Chandrasekhar, R. K. M. Raghupathy, K. H. Ly, H. Zhang, E. Dmitrieva and X. Feng, A high-rate two-dimensional polyarylimide covalent organic framework anode for aqueous Zn-ion energy storage devices, *J. Am. Chem. Soc.*, 2020, **142**, 19570–19578.
- 21 S. Xiong, X. Tang, C. Pan, L. Li, J. Tang and G. Yu, Carbazole-bearing porous organic polymers with a mulberry-like morphology for efficient iodine capture, *ACS Appl. Mater. Interfaces*, 2019, **11**, 27335–27342.
- 22 Q. Sun, Y. Tang, B. Aguila, S. Wang, F. S. Xiao, P. K. Thallapally and S. Ma, Reaction environment modification in covalent organic frameworks for catalytic performance enhancement, *Angew. Chem., Int. Ed.*, 2019, **58**, 8670–8675.
- 23 D. Wu, F. Xu, B. Sun, R. Fu, H. He and K. Matyjaszewski, Design and preparation of porous polymers, *Chem. Rev.*, 2012, **112**, 3959–4015.
- 24 S. Zhang, Q. Yang, C. Wang, X. Luo, J. Kim, Z. Wang and Y. Yamauchi, Porous organic frameworks: advanced materials in analytical chemistry, *Adv. Sci.*, 2018, **5**, 1801116.
- 25 E. Troschke, S. Grätz, T. Lübken and L. Borchardt, Mechanochemical Friedel–Crafts alkylation—a sustainable pathway towards porous organic polymers, *Angew. Chem., Int. Ed.*, 2017, **56**, 6859–6863.
- 26 C. Song, J. Nie, C. Ma, C. Lu, F. Wang and G. Yang, 1, 2, 3-Triazole-based conjugated porous polymers for visible light induced oxidative organic transformations, *Appl. Catal., B*, 2021, **287**, 119984.
- 27 Y. Mohr, M. Alves-Favaro, R. Rajapaksha, G. Hisler, A. Ranscht, P. Samanta and J. Canivet, Heterogenization of a Molecular Ni Catalyst within a Porous Macroligand for the Direct C–H Arylation of Heteroarenes, *ACS Catal.*, 2021, **11**, 3507–3515.
- 28 D. Ma, J. Li, K. Liu, B. Li, C. Li and Z. Shi, Di-ionic multifunctional porous organic frameworks for efficient CO₂ fixation under mild and co-catalyst free conditions, *Green Chem.*, 2018, **20**, 5285–5291.
- 29 K. Huang, J. Y. Zhang, F. Liu and S. Dai, Synthesis of porous polymeric catalysts for the conversion of carbon dioxide, *ACS Catal.*, 2018, **8**, 9079–9102.
- 30 J. Yu, X. Sun, X. Xu, C. Zhang and X. He, Donor-acceptor type triazine-based conjugated porous polymer for visible-light-driven photocatalytic hydrogen evolution, *Appl. Catal., B*, 2019, **257**, 117935.
- 31 A. E. Vilian, R. Sivakumar, Y. S. Huh, J. H. Youk and Y. K. Han, Palladium supported on an amphiphilic triazine–urea-functionalized porous organic polymer as a highly efficient electrocatalyst for electrochemical sensing of rutin in human plasma, *ACS Appl. Mater. Interfaces*, 2018, **10**, 19554–19563.
- 32 (a) M. Torabi, M. Yarie, M. A. Zolfigol, S. Azizian and Y. Gu, A magnetic porous organic polymer: catalytic application in the synthesis of hybrid pyridines with indole, triazole and sulfonamide moieties, *RSC Adv.*, 2022, **12**, 8804–8814; (b) M. Bayatani, M. Torabi, M. Yarie, M. A. Zolfigol and Z. Farajzadeh, Fabrication of an imidazolium-based magnetic ionic porous organic polymer for efficient heterogeneous catalysis of Betti reaction, *J. Mol. Liq.*, 2023, **390**, 122863–122871; (c) Z. Alishahi, M. Torabi, M. A. Zolfigol and M. Yarie, Nanoarchitectonics of magnetic covalent organic framework with sulfonic acid tags for catalytic preparation of triazolo quinazolinones and 4H-pyrimidobenzothiazoles, *J. Solid State Chem.*, 2023, **324**, 124119; (d) M. Torabi, M. A. Zolfigol and M. Yarie, Construction of a new 2D coral-like covalent organic framework as CuI nanoparticles carrier for the preparation of diverse triazoles, *Arab. J. Chem.*, 2023, **16**, 105090–105104; (e) A. Sanjabi, S. Azizian, M. Torabi, M. A. Zolfigol and M. Yarie, On the applicability of triazine-based



- covalent organic polymer as adsorbent for dye removal from aqueous solution, *Microporous Mesoporous Mater.*, 2023, **348**, 112367–112376.
- 33 X. Lan, Q. Li, Y. Zhang, Q. Li, L. Ricardez -Sandoval and G. Bai, Engineering donor-acceptor conjugated organic polymers with boron nitride to enhance photocatalytic performance towards visible-light-driven metal-free selective oxidation of sulfides, *Appl. Catal., B*, 2020, **277**, 119274.
 - 34 C. Zhao, C. S. Diercks, C. Zhu, N. Hanikel, X. Pei and O. M. Yaghi, Urea-linked covalent organic frameworks, *J. Am. Chem. Soc.*, 2018, **140**, 16438–16441.
 - 35 M. A. Ziaee, Y. Tang, H. Zhong, D. Tian and R. Wang, Urea-functionalized imidazolium-based ionic polymer for chemical conversion of CO₂ into organic carbonates, *ACS Sustain. Chem. Eng.*, 2018, **7**, 2380–2387.
 - 36 B. Atashkar, M. A. Zolfigol and S. Mallakpour, Applications of biological urea-based catalysts in chemical processes, *Mol. Catal.*, 2018, **452**, 192–246.
 - 37 J. Hu, F. Zanca, P. Lambe, M. Tsuji, S. Wijeweera, S. Todisco and H. Beyzavi, (Thio) urea-Based Covalent Organic Framework as a Hydrogen-Bond-Donating Catalyst, *ACS Appl. Mater. Interfaces*, 2020, **12**, 29212–29217.
 - 38 B. Dong, W. J. Wang, Y. Yang, R. Wang and S. C. Xi, One-Pot Synthesis of Deep Eutectic Solvents Containing Three-Dimensional Polymeric Materials with Excellent Catalytic Activity in the Knoevenagel Condensation Reaction, *ACS Appl. Polym. Mater.*, 2022, **4**, 8092–8097.
 - 39 C. Yadav, V. K. Maka, S. Payra and J. N. Moorthy, Multifunctional porous organic polymers (POPs): inverse adsorption of hydrogen over nitrogen, stabilization of Pd (0) nanoparticles, and catalytic cross-coupling reactions and reductions, *J. Catal.*, 2020, **384**, 61–71.
 - 40 J. Zhang, X. Han, X. Wu, Y. Liu and Y. Cui, Multivariate chiral covalent organic frameworks with controlled crystallinity and stability for asymmetric catalysis, *J. Am. Chem. Soc.*, 2017, **139**, 8277–8285.
 - 41 N. Haque, S. Biswas, P. Basu, I. H. Biswas, R. Khatun, A. Khan and S. M. Islam, Triazinetriamine-derived porous organic polymer-supported copper nanoparticles (Cu-NPs@ TzTa-POP): an efficient catalyst for the synthesis of *N*-methylated products via CO₂ fixation and primary carbamates from alcohols and urea, *New J. Chem.*, 2020, **44**, 15446–15458.
 - 42 M. Yarie, Spotlight: COFs as catalyst in organic methodologies, Iran, *J. Catal.*, 2021, **11**, 89–93.
 - 43 E. Valiey and M. G. Dekamin, Design and characterization of a urea-bridged PMO supporting Cu (II) nanoparticles as highly efficient heterogeneous catalyst for synthesis of tetrazole derivatives, *Sci. Rep.*, 2022, **12**, 18139.
 - 44 R. Pandey, D. Singh, N. Thakur and K. K. Raj, Catalytic C–H Bond Activation and Knoevenagel Condensation Using Pyridine-2, 3-Dicarboxylate-Based Metal–Organic Frameworks, *ACS Omega*, 2021, **6**, 13240–13259.
 - 45 A. A. Raza, S. Ravi, S. S. Tajudeen and A. I. Sheriff, Trifunctional covalent triazine and carbonyl based polymer as a catalyst for one-pot multistep organic transformation, *React. Funct. Polym.*, 2021, **167**, 105011.
 - 46 A. Samui, N. Kesharwani, C. Halder and S. K. Sahu, Fabrication of nanoscale covalent porous organic polymer: an efficacious catalyst for Knoevenagel condensation, *Microporous Mesoporous Mater.*, 2020, **299**, 110112.
 - 47 P. Sarma, K. K. Sarmah, D. Kakoti, S. P. Mahanta, N. M. Adasooriya, G. Nandi and R. Thakuria, A readily accessible porous organic polymer facilitates high-yielding Knoevenagel condensation at room temperature both in water and under solvent-free mechanochemical conditions, *Catal. Commun.*, 2021, **154**, 106304.
 - 48 Y. Wang, L. Wang, C. Liu and R. Wang, Benzimidazole-Containing Porous Organic Polymers as Highly Active Heterogeneous Solid-Base Catalysts, *ChemCatChem*, 2015, **7**, 1559–1565.
 - 49 P. Puthiaraj, Y. M. Chung and W. S. Ahn, Dual-functionalized porous organic polymer as reusable catalyst for one-pot cascade CC bond-forming reactions, *Mol. Catal.*, 2017, **441**, 1–9.
 - 50 M. Chaudhary and P. Mohanty, Nitrogen enrich polytriazine as a metal-free heterogeneous catalyst for the Knoevenagel reaction under mild conditions, *New J. Chem.*, 2018, **42**, 12924–12928.
 - 51 M. R. Anizadeh, M. A. Zolfigol, M. Yarie, M. Torabi and S. Azizian, Synthesis, characterization and catalytic application of tributyl (carboxymethyl) phosphonium bromotrichloroferrate as a new magnetic ionic liquid for the preparation of 2, 3-dihydroquinazolin-4 (1*H*)-ones and 4*H*-pyrimidobenzothiazoles, *Res. Chem. Intermed.*, 2020, **46**, 3945–3960.
 - 52 Y. Feng, Y. Li, G. Cheng, L. Wang and X. Cui, Copper-catalyzed synthesis of 2-arylquinazolinones from 2-arylindoles with amines or ammoniums, *J. Org. Chem.*, 2015, **80**, 7099–7107.
 - 53 M. Heidary, M. Khoobi, S. Ghasemi, Z. Habibi and M. A. Faramarzi, Synthesis of quinazolinones from alcohols via laccase-mediated tandem oxidation, *Adv. Synth. Catal.*, 2014, **356**, 1789–1794.
 - 54 M. L. Hu, V. Safarifard, E. Doustkhah, S. Rostamnia, A. Morsali, N. Nouruzi and K. Akhbari, Taking organic reactions over metal-organic frameworks as heterogeneous catalysis, *Microporous Mesoporous Mater.*, 2018, **256**, 111–127.
 - 55 K. Kulangiappar, M. Anbukulandainathan and T. Raju, Synthetic communications: an international journal for rapid communication of synthetic organic chemistry, *Synth. Commun.*, 2014, **1**, 2494–2502.
 - 56 S. Rostamizadeh, M. Nojavan, R. Aryan, E. Isapoor and M. Azad, Amino acid-based ionic liquid immobilized on α -Fe₂O₃-MCM-41: an efficient magnetic nanocatalyst and recyclable reaction media for the synthesis of quinazolin-4 (3*H*)-one derivatives, *J. Mol. Catal. A: Chem.*, 2013, **374**, 102–110.
 - 57 S. Rostamnia and E. Doustkhah, Nanoporous silica-supported organocatalyst: a heterogeneous and green



- hybrid catalyst for organic transformations, *RSC Adv.*, 2014, **4**, 28238–28248.
- 58 P. Salehi, M. Dabiri, M. A. Zolfigol and M. Baghbanzadeh, A new approach to the facile synthesis of mono- and disubstituted quinazolin-4 (3*H*)-ones under solvent-free conditions, *Tetrahedron Lett.*, 2005, **46**, 7051–7053.
 - 59 M. Dabiri, P. Salehi, M. Baghbanzadeh, M. A. Zolfigol, M. Agheb and S. Heydari, Silica sulfuric acid: an efficient reusable heterogeneous catalyst for the synthesis of 2, 3-dihydroquinazolin-4 (1*H*)-ones in water and under solvent-free conditions, *Catal. Commun.*, 2008, **9**, 785–788.
 - 60 M. A. Zolfigol, H. Ghaderi, S. Bagheri and L. Mohammadi, Nanometasilica disulfuric acid (NMSDSA) and nanometasilica monosulfuric acid sodium salt (NMSMSA) as two novel nanostructured catalysts: applications in the synthesis of Biginelli-type, polyhydroquinoline and 2, 3-dihydroquinazolin-4 (1*H*)-one derivatives, *J. Iran. Chem. Soc.*, 2017, **14**, 121–134.
 - 61 P. Salehi, M. Dabiri, M. A. Zolfigol and M. Baghbanzadeh, A novel method for the one-pot three-component synthesis of 2, 3-dihydroquinazolin-4 (1*H*)-ones, *Synlett*, 2005, 1155–1157.
 - 62 M. Shiri, M. M. Heravi, H. Hamidi, M. A. Zolfigol, Z. Tanbakouchian, A. Nejatinezhad-Arani and N. A. Koorbanally, Transition metal-free synthesis of quinolino [2', 3': 3, 4] pyrazolo [5, 1-*b*] quinazolin-8 (6*H*)-ones via cascade dehydrogenation and intramolecular *N*-arylation, *J. Iran. Chem. Soc.*, 2016, **13**, 2239–2246.
 - 63 A. Rostami, B. Atashkar and H. Gholami, Novel magnetic nanoparticles Fe₃O₄-immobilized domino Knoevenagel condensation, Michael addition, and cyclization catalyst, *Catal. Commun.*, 2013, **37**, 69–74.
 - 64 A. Ghorbani-Choghamarani, Z. Heidarneszhad, B. Tahmasbi and G. Azadi, TEDETA@ BNPs as a basic and metal free nanocatalyst for Knoevenagel condensation and Hantzsch reaction, *J. Iran. Chem. Soc.*, 2018, **15**, 2281–2293.
 - 65 R. F. Silver, K. A. Kerr, P. D. Frandsen, S. J. Kelley and H. L. Holmes, Synthesis and chemical reactions of some conjugated heteroenoid compounds, *Can. J. Chem.*, 1967, **45**, 1001–1006.
 - 66 S. Kotowicz, D. Sęk, S. Kula, A. Fabiańczyk, J. G. Małecki, P. Gnida and E. Schab-Balcerzak, Photoelectrochemical and thermal characterization of aromatic hydrocarbons substituted with a dicyanovinyl unit, *Dyes Pigm.*, 2020, **180**, 108432.
 - 67 M. Tarleton, L. Dyson, J. Gilbert, J. A. Sakoff and A. McCluskey, Focused library development of 2-phenylacrylamides as broad spectrum cytotoxic agents, *Bioorg. Med. Chem.*, 2013, **21**, 333–347.
 - 68 J. Quiroga, J. Trilleras, A. I. Sanchez, B. Insuasty, R. Abonia, M. Nogueras and J. Cobo, Regioselective three-component synthesis of indolylpyrazolo [3, 4-*b*] pyridines induced by microwave and under solvent-free conditions, *Lett. Org. Chem.*, 2009, **6**, 381–383.
 - 69 B. D. Rupanawar, S. M. Veetil and G. Suryavanshi, Oxidative olefination of benzylamine with an active methylene compound mediated by hypervalent iodine (III), *Eur. J. Org. Chem.*, 2019, **2019**, 6232–6239.
 - 70 P. Ondet, G. Lemi  re and E. Du  nach, Cyclisations catalysed by bismuth (III) triflate, *Eur. J. Org. Chem.*, 2017, **2017**, 761–780.
 - 71 R. J. Kalbasi and A. Khojastegi, Hierarchically Pore Structure poly 2-(Dimethyl amino) ethyl methacrylate/Hi-ZSM-5: A Novel Acid-Base Bi-functional Catalyst as Heterogeneous Platform for a Tandem Reaction, *Catal. Lett.*, 2018, **148**, 958–971.
 - 72 M. Mohammadi and A. Ghorbani-Choghamarani, Complexation of guanidino containing L-arginine with nickel on silica-modified Hercynite MNPs: a novel catalyst for the Hantzsch synthesis of polyhydroquinolines and 2, 3-dihydroquinazolin-4 (1*H*)-ones, *Res. Chem. Intermed.*, 2022, **48**, 2641–2663.
 - 73 A. Dutta, K. Damarla, A. Bordoloi, A. Kumar and D. Sarma, KOH/DMSO: a basic suspension for transition metal-free tandem synthesis of 2, 3-dihydroquinazolin-4 (1*H*)-ones, *Tetrahedron Lett.*, 2019, **60**, 1614–1619.
 - 74 M. Prakash and V. Kesavan, Highly enantioselective synthesis of 2, 3-dihydroquinazolinones through intramolecular amidation of imines, *Org. Lett.*, 2012, **14**, 1896–1899.
 - 75 C. H. Liu, Q. Wang, Z. Xu, D. Li and Y. Zheng, 5, 5'-Indigodisulfonic acid as an efficient catalyst for the synthesis of 2, 3-dihydroquinazolinone derivatives, *Synth. Commun.*, 2022, **52**, 1537–1545.
 - 76 M. Hajjami, S. Sheikhaei, F. Gholamian and Z. Yousofvand, Synthesis and characterization of magnetic functionalized Ni and Cu nano catalysts and their application in oxidation, oxidative coupling and various multi-component reactions, *Catal. Lett.*, 2021, **151**, 2420–2435.
 - 77 N. Bu, W. Y. Wu, P. Jiang, Z. Y. Zhan, J. L. Wan, Z. J. Wu and R. Wan, Self-assembly and steric hindrance for further host-guest interactions of a tetrahedral cage Fe₄^{II}L₄, *Chem. Pap.*, 2021, **75**, 4493–4499.

